This document is confidential and is proprietary to the American Chemical Society and its authors. Do not copy or disclose without written permission. If you have received this item in error, notify the sender and delete all copies.

Preparation, characterization, and mechanism for biodegradable and biocompatible polyurethane shape memory elastomers

Journal:	*ACS Applied Materials & Interfaces*
Manuscript ID	am-2016-11993a.R2
Manuscript Type:	Article
Date Submitted by the Author:	21-Jan-2017
Complete List of Authors:	Chien, Yu-chun; Institute of Polymer Science and EngineeringNational, National Taiwan University Chuang, Wei-Tsung; National Synchrotron Radiation Research Center, Research Division Jeng, U-Ser; National Synchrotron Radiation Research Center, Facility Utilization Hsu, Shan-hui; National Taiwan University, Polymer Science and Engineering

SCHOLARONE™
Manuscripts

Preparation, characterization, and mechanism for biodegradable and biocompatible polyurethane shape memory elastomers

Yu-chun Chien[†], Wei-Tsung Chuang[‡], U.-Ser Jeng[‡], Shan-hui Hsu[*,†]

[†]Institute of Polymer Science and Engineering, National Taiwan University, Taipei, Taiwan

[‡]National Synchrotron Radiation Research Center, Hsinchu, Taiwan

***Shan-hui Hsu (Corresponding author)**

Institute of Polymer Science and Engineering, National Taiwan University, No. 1, Sec. 4 Roosevelt Road, Taipei 10617, Taiwan, R.O.C.

Phone: (886) 2-33665313

Fax: (886) 2-33665237

E-mail: shhsu@ntu.edu.tw

Abstract

Thermally induced shape memory is an attractive feature of certain functional materials. Among the shape memory polymers, shape memory elastomers (SMEs) especially those with biodegradability have great potential in the biomedical field. In this study, we prepared waterborne biodegradable polyurethane SME based on poly(ε-caprolactone) (PCL) oligodiol and poly(L-lactic acid) (PLLA) oligodiol as the mixed soft segments. The ratio of the soft segments in polyurethanes was optimized for shape memory behavior. The thermally induced shape memory mechanism of the series of polyurethanes was clarified using differential scanning calorimeter (DSC), X-ray diffraction (XRD), and small angle X-ray scattering (SAXS). In particular, the in situ SAXS measurements combined with shape deformation processes were employed to examine the stretch-induced (oriented) crystalline structure of the polyurethanes and to elucidate the unique mechanism for shape memory properties. The polyurethane with optimized PLLA crystalline segments showed a diamond-shape two-dimensional SAXS pattern after being stretched, which gave rise to better shape fixing and shape recovery. The shape memory behavior was further tested in 37 ℃ water. The biodegradable polyurethane comprising 38 wt% PCL segments and 25 wt% PLLA segments and synthesized at a relatively lower temperature by the waterborne procedure showed ~100% shape recovery in 37 ℃

water. The biodegradable polyurethane SME also demonstrated good endothelial cell viability as well as low platelet adhesion/activation. We conclude that the waterborne biodegradable polyurethane SME possesses a unique thermally induced shape memory mechanism and may have potential applications in making shape memory biodegradable stents or scaffolds.

Keywords: shape memory polyurethane, in situ SAXS, biodegradable, biocompatible, elastomer.

1. Introduction

Shape memory behavior is a unique property of a series smart materials having the ability to recover to the initial state from the deformed state upon sensing an external stimulus[1]. Due to this inductive characteristics, shape memory materials have potential applications in the biomedical field, such as orthopedic surgery[2], intracranial aneurysm[3], hemodialysis[4], thrombus removing[5], surgical suture[6], and facial reconstruction[7]. Shape memory materials can be classified to shape memory alloy (SMA) and shape memory polymer (SMP). SMA with high modulus show shape memory behavior by transformation between the martensitic state and austenitic state, and are used as orthopedic and dental implants. However, a second operation is needed to remove the implant from the patients because SMA medical devices cannot be decomposed in human body. In contrast, SMP can be equipped with biodegradable characteristics by introducing degradable molecular segments. Therefore, the SMP implants may gradually disappear from the surgical site as time proceeds. Additionally, SMPs are more cost-effective, and their physico-chemical properties are more tunable. There are many ways to trigger shape memory behavior including heat[8], light[9], ionic strength[10], moisture[11], and electromagnetic field[12]. Thermal stimulus is a straightforward candidate and provided directly by the human body temperature (near 37 °C). For this reason, the thermally responsive SMPs have been studied quite

extensively[13].

The heat induced SMPs can be classified into two categories based on different switching points. One of the switching points is the melting temperature (T_m)[14]. T_m based SMPs can be fixed at a temporary shape by forming crystal structure at a temperature lower than T_m. Once being heated over T_m, the crystalline region will melt slowly, and the SMP becomes soft enough to recover to the un-stretched state. Another switching point is the glass transition temperature (T_g)[15]. T_g based SMPs rely on the amorphous segment to perform fixing and recovery. When T_g based SMPs are heated over T_g, the SMP will transform from the glassy state to rubbery state, and gain more free volume to support the recovery.

To meet the degradation demand, the physical crosslinking (secondary forces) designed in SMPs is an appropriate strategy. The chemically crosslinked polymer structure on the other hand would take more time to degrade owing to the covalent bonding between polymer chains[16]. Therefore, many researchers have focused on making SMPs from linear polymers such as the systems of polyhedral oligomeric silsesquioxane (POSS)/polyethylene glycol (PEG)[11], poly(L-lactide-co-caprolactone) (PLCL)/poly (lactic-co-glycolicacid) (PLGA)[12], polycaprolactone (PCL)/polyethylene glycol (PEG)[17], and polycaprolactone (PCL)/poly-L-lactide (PLLA)[18].

To meet the requirement of biomedical uses, SMPs should also be biocompatible,

biodegradable, and can be designed to have tunable mechanical properties. For example, polyurethane, which is a category of elastomers, has received much attention as the candidate material for shape memory elastomers (SMEs) because of the manipulated crystallinity, thermal properties, and biocompatibility[19]. However, a biodegradable SME has been rarely reported in literature. Polyurethanes can be made biodegradable by selecting proper hard and soft segments[20]. Previously, we have developed a aqueous process to prepare biodegradable PCL-PLLA oligodiol based polyurethane[21]. In such a system, the crystallinity of polyurethane may further be fine-tuned by applying different prepolymerization temperatures and soft segment compositions. In this work, we synthesized a series of PCL-PLLA oligodiol based polyurethanes. We proposed that the PCL crystallized structure in polyurethanes may provide T_m as the switching point, while the PLLA crystallized structure in polyurethanes may offer T_g as another possible switching point for development of SMEs. By adjusting the ratio between PCL and PLLA soft segments, we expected to optimize the formula for biodegradable polyurethane SME and evaluate the shape memory behavior. In particular, the in situ small angle X-ray scattering (SAXS) combining a tensile machine was employed to examine the shape memory mechanism and clarify which switching point contributed to the shape memory property.

2. Materials and Methods

2.1. Materials

Poly(ε-caprolactone) diol (number-average molecular weight 2000) was purchased from Sigma-Aldrich. Poly(L-lactic acid) diol (number-average molecular weight 2000) was synthesized by ring opening polymerization of L-lactide monomer (Purac, Netherland) and 1, 3-propane diol (Alfa, Aesar) with the catalysis of stannous octoate ($Sn(Oct)_2$) (Alfa, Aesar). Isophorone diisocyanate was purchased from Acros. 2, 2-Bis(hydroxymethyl) propionic acid (DMPA) and trimethylamine (TEA) were purchased from Sigma-Aldrich. Ethylenediamine (EDA) was purchased from Tedia, USA.

2.2. Synthesis of polyurethanes

Polyurethanes were synthesized by the following steps with some modification based on literature[21]. Poly(ε-caprolactone) diol and poly(L-lactic acid) diol were poured into a four neck round bottle in various ratios (PCL:PLLA 1:0, 8:2, 7:3, 6:4. And 5:5). Polyurethanes synthesized were named PCL100, PCL80LL20, PCL70LL30, PCL60LL40 and PCL50LL50, respectively. The system temperature was held at either 75 °C (PCL100, PCL70LL30, PCL60LL40 and PCL50LL50) or 95 °C (PCL80LL20, PCL70LL30, PCL60LL40 and PCL50LL50) and was purged with

nitrogen to well mix the oligodiols and prevent humidity from interfering with the reaction. The stirring speed was set up at 180 rpm. After purging and stirring for 30 min, the catalyst (0.05wt% of polyurethane) was added to the oligodiols and then 4.18 g isophorone diisocyanate (well-mixed in ologodiols) was dropped into the system to initiate the prepolymerization for 3 h. After that, DMPA (acidic ionizer) was put into the system with a certain amount of methyl ethyl ketone (lubricant) to ionize the polyurethane at 75°C for 1 h. Subsequently, TEA as a basic neutralizer was added to pull out the negative charge on DMPA. Finally, EDA (chain extender) water solution was dropwise added to the system with strong mechanical stirring (1150 rpm). The polyurethane dispersions thus prepared were cast on Teflon molds into films and the residual solvent was removed by vacuum for 24 h. All the samples presented in this work were polyurethane solid films after complete water removal. The synthesis procedure is shown in Figure S1.

2.3. Physico-chemical characterization

Differential scanning calorimetry (DSC, Q20, TA universal, USA) was performed to measure the crystallinity and melting point of the polyurethanes. Each sample was heated from −70 °C to 130 °C with a heating rate of 10°C/min under nitrogen purging. The pan and lid were aluminum. The samples weighed about 5 mg

for each measurement.

The diffraction peaks of each polyurethane were obtained using an X-ray diffractometer (XRD, X'Pert, PANalytical, Netherland) with Cu Kα radiation (40kV, 40mA). The intensity was detected from 10° to 30° at a speed of 0.02°/s under room temperature. The calculation method of crystallinity is shown in Figure S2.

2.4. Small angle X-ray scattering (SAXS)

The microstructures of polyurethane films were investigated by SAXS at the beamline 23A of the National Synchrotron Radiation Research Center at Hsinchu, Taiwan. The photon energy was at about 10 keV. The range of scattering vector was from 0.002 to 0.2 $Å^{-1}$, and the cell temperature was raised from 30 °C to 120 °C.

2.5. Shape memory behavior in air

The shape memory properties were measured by the bending test shown in Figure 2A in two cycles. Each sample was 40 mm (length) × 5 mm (width) × 0.2 mm (thickness) in size. The test was conducted in four steps as described below. First, the sample was deformed to the U shape in a 50 °C vacuum oven. Second, the U shape sample was fixed in a refrigerator at −18 °C for 5 min. Third, the sample was placed in a refrigerator at 0 °C for 5 min, and the angle after fixing (θ_1) was measured.

Finally, the sample was put into 50 °C vacuum oven or 37 °C vacuum oven for different recovery conditions for 5 min, and the angle after recovery (θ_B) was measured. The same procedure was repeated again once. θ_A and θ_B were measured after maintaining for 1 min at room temperature (25 °C). The shape fixing ratio and the shape recovery ratio are defined from θ_A and θ_B, respectively, as shown below.

$$\text{Shape fixity ratio } (\%) = \frac{\theta_A}{180} \times 100 \quad \text{.....(1)}$$

$$\text{Shape recovery ratio } (\%) = \frac{180-\theta_B}{180} \times 100 \quad \text{.....(2)}$$

2.6. In situ SAXS and WAXS

To perceive the transformation of microstructure under shape memory procedure (Figure 2B), the in situ small angle X-ray scattering (SAXS) and wide angle X-ray scattering (WAXS) experiments were performed at the beamline 23A of the National Synchrotron Radiation Center at Hsinchu, Taiwan. The wavelength of radiation was 0.154 nm. The photon energy was 10 keV. The range of scattering vector was from 0.002 to 0.2 $Å^{-1}$. There were three different patterns each obtained at the initial, stretched, and recovery states. The initial state was the state before stretching. The switching temperature tensile machine was equipped to stretch polyurethane films to 50% strain at 50 °C, and then cooled to 0 °C to fix the temporary shape (stretched state). Finally, the temperature was raised to 50 °C (recovery state). The SAXS and

WAXS measurements were taken in 200 s and 10 s per shot respectively in the deforming process.

2.7. Shape memory behavior in water

To evaluate the recovery ratio affected by water, the recovery environment was changed to 25 ℃ or 37 ℃ water. The sample was 40 mm (length) × 5 mm (width) × 0.2 mm (thickness) in size. The deforming procedure was the same as that described in Sec. 2.5. After fixing the U shape, the sample was immersed into the water (25 ℃ or 37 ℃) for 5 min, and the angle after recovery (θ_B) was measured. The recovery ratio was calculated by eq (2). In another experiment, the polyurethane film was twisted to form a spiral shape at 50 ℃, cooled to -18 ℃ to fix, and then the polyurethane was immersed in 37 ℃ water.

2.8. Infrared analysis

The attenuated total reflectance-Fourier transform infrared (ATR-IR) spectra were acquired by an infrared spectrometer (SP100, Perkin Elmer, USA). The absorbance was collected at a range of 1350-4000 cm^{-1} with a resolution of 4 cm^{-1}. The absorbance peaks associated with free C=O and hydrogen-bonded C=O were quantified to determine the effect from the hydrogen bond. ATR-IR spectra were

collected for the original dry samples as well as for those immersed in water for 5 min, wiped, and immediately measured after purging.

2.9. Mechanical properties

The tensile stress, tensile strain, and 100% modulus of dry and wet samples were examined using a tensile tester (HT-8504, Hung Ta, Taiwan). Polyurethane films were cut into dog-bone shape by a cutting mold. The specimen dimensions were 20 mm (length) × 4.7 mm (width) × 0.2mm (thickness) in size. The stretching speed was set at 100 mm/min (ASTMD638.10 for elastomers). The wet sample was immersed in water for 5 min, wiped by lens paper to remove water on the film surface, and immediately measured by the tensile tester.

2.10. Cell viability and blood compatibility of polyurethane films

Bovine endothelial cells (ECs) were used to characterize the cytocompatibility and cell proliferation on biodegradable polyurethanes that included PCL100, PCL80LL20, and PCL60LL40, and on Pellethane® 2363-80AE TPU (commercial biomedical grade non-biodegradable polyurethane) that served as a control material. The culture medium consisted of low-glucose Dulbecco's modified Eagle's medium (DMEM, Gibco), 10% fetal bovine serum (FBS, gibco), 1% penicillin streptomycin

(Gibco), 3.7 g/L sodium bicarbonate ($NaHCO_3$, Sigma). The incubator was maintained at 37 °C with 5% CO_2. ECs were loaded in 24 well cell culture plates with 4×10^4 cells/well and incubated for 24 h and 72 h. The cell viability was evaluated using the 3-(4,5-dimethylthiazol-2-yl)-2,5-diphenyltetrazolium bromide (MTT) assay. The value of cell viability was obtained by normalization to a blank well at 24 h. Platelets acquired from the blood of Sprague-Dawley rat were used to examine the blood compatibility of polyurethanes. The platelets were seeded on the polyurethanes and incubated for 1 h. After incubation, the samples were fixed with 2.5% glutaraldehyde for 3 h. The samples were dehydrated in gradient ethanol from 60%, 65%, 70%, 75%, 80%, 85%, 90%, 95%, to 99.5% for 10 min each, and critical point dried. The morphology of platelets on polyurethanes was observed with a scanning electron microscope (SEM, Hitachi, TM3000, Japan).

3. Results

3.1. Optimization of the ratio of PCL and PLLA soft segments in polyurethanes

First, we compared the properties of six different polyurethanes synthesized at two different prepolymerization temperatures, i.e. PCL70LL30 (75 °C), PCL70LL30 (95 °C), PCL60LL40 (75 °C), PCL60LL40 (95 °C), PCL50LL50 (75 °C), and PCL50LL50 (95 °C). The crystallinity of these polyurethanes was examined by DSC

(Figure S2) and XRD (Figure S3). The DSC curve of PCL60LL40 (75 °C) showed a distinct endothermic peak between 120 °C and 130 °C. It appeared that the broad melting peak was a combination of two peaks. The same tendency was observed in the other samples, but not as obvious. There were small noises (less than 0.1 J/g) below 100 °C probably owing to the presence of a small part of PLLA oligodiol with lower molecular weight (less than 2000). The quantified results are listed in Table S1. PCL60LL40 (75 °C) had the largest melting heat. The enthalpy of fusion from DSC curves (an index for crystallinity) was enhanced as the PCL/PLLA soft segment ratio decreased from 7:3 (PCL70LL30) to 6:4 (PCL60LL40) while significantly reduced as the ratio decreased from 6:4 to 5:5 (PCL50LL50). The effect of prepolymerization temperature (75 or 95 °C) on fusion enthalpy was not evident except for PCL60LL40.

To verify the data of DSC, the XRD experiment was carried out (Figure S3). The XRD patterns for all six polyurethanes revealed two sharp peaks representing the PLLA crystals at around 16.5° and 18.9°[22]. The obscure peaks around 21° and 23° were related to PCL crystals[21]. As the PLLA content was increased to 50% in polyurethanes [PCL50LL50 (75 °C)], the PCL peaks in the XRD pattern was more visible. All polyurethanes showed clear PLLA peaks by XRD. Among them, PCL60LL40 (75 °C) had the sharpest diffraction peaks. The degree of crystallinity calculated based on XRD curves is listed in Table S2. PCL60LL40 (75 °C) had about

10% crystallinity attributed to the PLLA segment in the structure. This outcome was consistent with that observed by DSC.

The microstructure of polyurethanes was further analyzed using SAXS. The scattering profiles (Kratky plots) are demonstrated in Figure S4. All samples revealed a bell-shaped SAXS pattern around q=0.06 $Å^{-1}$. Compared to polyurethanes synthesized at 95 °C, the polyurethanes prepared with a lower polymerization temperature (75 °C) showed more scattering peaks. As the testing temperature rose, all the scattering peaks and bell-shaped patterns tended to be flattened. Moreover, the Kratky plots (Figure S4) exhibited a drastic upshift to higher intensities at the high q range. In particular, PCL60LL40 (75 °C) had Iq^2 peaks with the integer ratios of q values at q=0.017, 0.034, and 0.051 $Å^{-1}$. This observation suggests that PCL60LL40 (75 °C) may have lamellar crystalline structure, which is typical of some polyurethanes[23].

Based on the above study, we selected PCL60LL40 synthesized at 75 °C (with ~10% PLLA crystallinity) as the possible formula for biodegradable SME, and further compared it with PCL100 (amorphous) and PCL80LL20 (with ~10% PCL crystallinty) to establish the mechanism for shape memory behavior.

3.2. Crystallinity analysis for PCL100, PCL80LL20, and PCL60LL40

Starting from here, comparison was made between PCL100, PCL80LL20, and PCL60LL40 (75 °C). PCL60LL40 (75 °C) will be presented in short abbreviation as PCL60LL40. As shown in Figure 1A, DSC curves for these polyurethanes displayed no exothermic peaks during the heating process, i.e. no re-crystallization. Among the samples, PCL100 had an evident glass transition point at -49°C, but showed no melting peak. This indicated that PCL100 was an amorphous polyurethane. The glass transition point could not be detected for both PCL80LL20 and PCL60LL40, but their curves showed an endothermic pattern which was different for each polymer. PCL80LL20 demonstrated a broad peak around 45 °C that was referred to the crystallization of PCL. The endotherm transition around 80 °C was probably due to the chain alignment of hard segment. On the contrary, PCL60LL40 without the PCL endothermic peak showed the combination of two PLLA peaks around 120 °C. The XRD experiment was performed to verify the results of DSC and the data are presented in Figure 1B. PCL100 displayed a classic amorphous broad band centering at 18° and ranging from 10° to 30°. PCL80LL20 showed two diffraction peaks at 21° and 23° associated with PCL crystal (10% crystallinity), and a small diffraction peak at 16.5° associated with PLLA crystal (1% crystallinity). PCL60LL40 exhibited two PLLA diffraction peaks at 16.5° and 18.9° (10% crystallinity). The respective crystallinity of polyurethanes is listed in Table 1. According to the analyses, we

proposed that PCL80LL20 and PCL60LL40 were close in the overall degree of crystallinity.

3.3. Shape memory properties of polyurethanes in air

The ratios of shape memory fixity (performed at -18 °C) and the shape memory recovery (performed at 50 °C) determined at 25°C (Figure 2A) are listed in Table 2. PCL100 had an excellent recovery ratio (~100%, 3 s) but poor fixing ability (~36%). With the addition of PLLA, PCL80LL20 possessed good shape fixing capability (~100%) while lost the recovery ability (~38%, 5 min). With the PLLA content being 40%, PCL60LL40 had a higher shape fixing ratio (~75%) than PCL100, as well as a higher shape recovery ratio (~87%, 72 s) than PCL80LL20. In the cycle 2 of the shape memory experiment, all samples revealed better shape memory fixity ratios, and slightly declined shape recovery ratios.

3.4. In situ SAXS/WAXS analysis

The shape deforming process by a tensile tester during the in situ SAXS/WAXS measurements is illustrated in Figure 2B. The in situ scattering patterns collected during the shape memory process through the combination of synchrotron radiation and the tensile tester are demonstrated in Figure 3. At the initial state, the samples

were untreated. In the stretched state, the sample was deformed to 50% strain under 50 °C, and cooled to -18 °C to maintain the deformation. In the recovery state, the sample was heated to 50 °C to recover. As shown in Figure 3A, PCL100 presented a circular SAXS pattern at the initial and recovery states. Meanwhile, the SAXS pattern after stretching was transformed from the circle to an ellipse. Simultaneously, the broad amorphous band disappeared in the WAXS pattern after stretching. After recovery, the broad amorphous band showed up again. For PCL80LL20 at the initial state, the WAXS pattern (Figure 3B) showed a PLLA peak at 9° (2.93% crystallinity) and three PCL peaks at 11.5°, 12.5°, and 15.6° (each with 9.45%, 2.66%, and 2.93% crystallinity). The SAXS pattern of PCL80LL20 was also circular at the initial state. In the stretched state, the PCL peaks in the WAXS pattern of PCL80LL20 merged to a new PCL peak at 14.5° (5.52% crystallinity), and the PLLA peak became stronger (3.54% crystallinity). Besides, the SAXS pattern showed a shape between a diamond and an ellipse. After recovery, the PCL peak in the WAXS pattern of PCL80LL20 at 14.5° (4.07% crystallinity) still existed, but the PLLA peak at 9° (2.30% crystallinity) was relatively smaller. Unexpectedly, there was a small new peak related to PLLA appearing near 10.3° (0.91% crystallinity). The SAXS pattern of PCL80LL20 after recovery displayed an ellipse shape. For PCL60LL40 at the initial state, SAXS exhibited a circular pattern, and WAXS showed clear PLLA peaks at 13° (7.86%

crystallinity) and 16° (2.30% crystallinity). After stretching, the circle in the SAXS pattern of PCL60LL40 turned to an apparent diamond shape. Also, the peak at 13° in the WAXS pattern of PCL60LL40 became sharper (11.21% crystallinity), and the peak at 16° was smaller (1.52% crystallinity). Furthermore, the intensity of amorphous band decayed. After recovery, the SAXS pattern of PCL60LL40 remained the diamond shape. The WAXS peak of PCL60LL40 at 13° was not significantly affected by the recovery process, while the WAXS peak at 16° declined (1.14% crystallinity). In summary, the diamond shape SAXS pattern of PCL60LL40 was related to the PLLA segment in the structure, and closely associated with its shape memory behavior.

3.5. Shape recovery of polyurethane in 37 °C water

For medical applications, the switching condition should be 37 ℃ water instead of 50 ℃ air. We conducted the shape memory recovery in 37 ℃ water bath (but unable to perform in situ SAXS). A comparison of the recovery ratio and recovery time in different conditions is summarized in Table 3. In 37 ℃ air, the shape recovery ratio of PCL60LL40 dropped to 71% from 87% in 50 ℃ air. The shape recovery ratio was 65% in 25 ℃ water, and elevated to 100% in 37 ℃ water (Figure 4A). In addition, the recovery from the U shape to the initial flat shape was very fast (~100%

in 20 s). To prove the recovery was useful, Figure 4B demonstrates the recovery of the spiral polyurethane (PCL60LL40) ribbon after immersion in 37 ℃ water. The multi-spiral shape was resolved in 20 s.

3.6. Influence of water verified by the mechanical and infrared analyses

The improvement of shape memory for PCL60LL40 in the presence of water was explained based on the influence of water. Mechanical properties and ATR-IR spectra may provide information regarding the kinetic and thermodynamic rationale for the improved recovery in water. The stress-strain curves of all polyurethanes are shown in Figure S6. The stress-strain curves of PCL60LL40 in the dry and wet states are shown in Figure 5A. The tensile strength, elongation at break, Young's modulus, and 100% modulus are listed in Table S3. In the dry state, PCL60LL40 showed ~11.04 MPa tensile strength and ~384% elongation at break. After immersion in water, the tensile strength was slightly decreased to ~10.01 MPa, but the elongation at break was significantly elevated to ~546%. The Young's modulus and 100% modulus also declined. This indicated that the polyurethane SME (PCL60LL40) became more flexible through interaction with water.

ATR-IR spectroscopy was employed to verify the interaction of water with the polyurethane. The spectra of all polyurethanes are shown in Figure S7. The spectrum

of PCL60LL40 in the original state and that immediately measured after immersion in water, removed, and dried are shown in Figure 5B. The major peaks in PCL60LL40 included 3360 cm^{-1} (N-H stretching), 2943 cm^{-1} (asymmetric C-H stretching), and 2866 cm^{-1} (symmetric C-H). No peak appeared at 2270 cm^{-1} (N=C=O), pointing out the absence of unreacted isocyanate group. The difference in spectra between the original state and the state after immersion lied in the C=O band near 1643 cm^{-1}. The unbound C=O of urethane was observed at 1731 cm^{-1} and 1757 cm^{-1} (PCL and PLLA soft segment). The hydrogen-bonded C=O was located at 1643 cm^{-1} (urethane group, urea group, and DMPA). In the original state, the peak at 1643 cm^{-1} was not evident. Based on calculation of bound and unbound C=O, the original PCL60LL40 had 32.4% hydrogen-bonded C=O. After immediately immersion, the peak at 1643 cm^{-1} was smaller and the fraction of hydrogen-bonded C=O dropped to 24.4%. This suggested that water molecule may compete for hydrogen-bonded C=O to exert physical interaction between water and SME and to favor shape recovery.

3.7. Endothelial cell (EC) attachment and proliferation

The attachment and the proliferation of ECs are shown in Figure 6A. After cell culture on polyurethanes for 24 h, the cell viability was in similar levels for all samples, demonstrating that ECs could attach on all polyurethanes. The cell viability

increased after 72 h, indicating that the polyurethanes had no cytotoxicity. For blank TCPS, the cell viability increased from ~125% (24 h) to ~300% (72 h). Cells on Pellethane proliferated from 24 h to 72 h and had the greatest viability at 72 h among all samples. For the synthesized polyurethanes, only PCL60LL40 showed a significant increase in the cell viability from 24 h to 72 h. The latter suggested that ECs proliferate better on PCL60LL40 than on PCL100 or PCL80LL20.

3.8. Blood compatibility

The morphology of platelets adhered on various polyurethanes after 1 h of contact is displayed in Figure 6B, and the average degree of adhesion and activation are summarized in Table S4. The platelets on Pellethane extended their pseudopodium to reach the other platelets, and the shape of platelets was flat, which were signs of activation. On PCL100 and PCL80LL20, the platelets also spread. However, the number of adhered platelets on PCL100 and PCL80LL20 was smaller and the platelets were not entangled with each other. On PCL60LL40, the platelets remained more spherical in shape. In addition, the surface of PCL60LL40 revealed little adhesion of leukocytes and erythrocytes, as well as the least number of platelets compared to the other samples.

4. Discussion

Polyurethane dispersions were synthesized with a waterborne process to diminish the use of organic solvent. Polyurethane films could be conveniently prepared by casting. In a previous study, we observed that the waterborne polyurethane consisting of 100% PCL (Mw 2000) soft segment (PCL100) was amorphous, while that consisting of 80% PCL soft segment and 20% PLLA (Mw 2000) soft segment (PCL80LL20) presented some crystalline PLLA as well as crystalline PCL structure[21]. Therefore, PCL80LL20 could be regarded as switchable polyurethane because of the presence of PCL crystalline domain, while PCL100 was a polyurethane without any switching possibility. To verify the shape memory ability of PCL segment and PLLA segment, in this study we further developed polyurethanes with possibly similar switching based on PLLA crystalline domain. The phase mixing/separation of PCL and PLLA oligodiols was further manipulated by changing the prepolymerization temperatures (75 ℃ and 95 ℃) and the ratios between the oligodiols soft segment (PCL/PLLA 7:3, 6:4, and 5:5). The thermal behavior and heat of fusion were first determined by DSC. All polyurethanes revealed a broad peak near 120-130 ℃, which we proposed as the overlap of two PLLA peaks. The sample PCL60LL40 (75 ℃) showed the sharpest endothermic peak and the highest melting temperature. This implied higher crystallinity of the sample. The crystallinity of these

polyurethanes was verified by XRD data. Polyurethanes with a higher PCL content displayed no diffraction peak of PLLA (16.5°/18.5°) [PCL70LL30 (95 °C)] or obscure peak of PLLA [PCL70LL30 (75 °C)]. As the PLLA content increased, the PLLA peak at 18.5° took shape and turned clear. Meanwhile, PCL60LL40 had the highest crystallinity instead of the polyurethane with a greater content of PLLA (i.e. PCL50LL50). Based on these observations, both the composition and prepolymerization temperature influenced the degree of crystallinity. The prepolymerization temperature affected the miscibility of PCL and PLLA segments due to distinct melting points of these two oligodiols. Therefore, the prepolymerization temperature may also affect the mobility of PLLA segment. We assumed that at 95 °C, the crystalline PLLA oligodiol may melt (more mobile), and be more difficult to rearrange (crystallize) during synthesis. Taken together, the data supported that PCL60LL40 (75 °C) had a degree of crystallinity ~10% close to that of PCL80LL20. SAXS profiles of the polyurethanes confirmed that the intensity climbed upward at the high q range as the temperature rose. This meant that the polyurethane chains turned less tight and became flexible at higher temperatures. Moreover, polyurethanes prepolymerized at 75 °C had more scattering peaks than those at 95 °C, which suggested that the former polyurethanes were easier to form organized structure. In particular, PCL60LL40 (75 °C) was distinctive for the scattering peaks in integer

ratios, which stood for a lamellar structure. Therefore, PCL60LL40 (75 °C) was a good candidate to contrast PCL100 and PCL80LL20 and to elucidate the shape memory mechanism of the waterborne/biodegradable polyurethane SME.

Based on the shape memory testing in air, PCL100 without crystalline structure (no switching segment) had a low fixing ratio and an excellent recovery ratio. This inability to retain the deformed shape is typical of a regular elastomer. Still, the feature of elasticity (rebound quickly on heating) offered some advantage to shape memory. Adding 20% PLLA segment significantly improved the fixing ratio but sacrificed the inherent recoverable properties of amorphous PCL segments. By examining the crystallinity of this polyurethane (PCL80LL20), we suggested that the failure in simultaneously keeping the fixing and recovery was attributed to the dual but conflicting roles of PCL. The amorphous PCL segments helped heat recovery while the crystalline PCL segments facilitated fixing under freezing. To achieve a good fixing ratio without sacrificing recovery, we proposed that the fixing segment may not also serve as the recovery segment in the polyurethane SME. In the optimized shape memory sample PCL60LL40, we expected that the crystalline PLLA segment to resolve the conflicting role of PCL segment. As a matter of fact, the shape memory properties were significantly improved in PCL60LL40. To test our

hypothesis, an in situ SAXS/WAXS combined with the shape memory test was performed.

The results from the in situ synchrotron measurement shed lights on the possible shape memory mechanism of the biodegradable polyurethane SME. To our surprise, the mechanism was different from or more sophisticate than the hypothesis described in the previous paragraph. PCL100, when elongated, formed an oriented crystalline (upright ellipse in SAXS). The broad amorphous halo detected in WAXS became vanished with a little peak at 12°, which was possibly the oriented PCL segment. This observation implied that the irregular chains tended to shorten their distance and thereby increase van der Waals' interaction and fix the temporary shape. Nonetheless, the amorphous halo reappeared after recovery. The ordered structure probably existed for a moment upon stretching. As the stress was removed, the aligned PCL segment returned to isotropic, and the 2D SAXS pattern showed a circle. The transformation of SAXS and WAXS suggested that the amorphous PCL segments in polyurethane was responsible for recovery, and the fixing element should be sought for another. For PCL80LL20 at the initial state, the WAXS pattern revealed a small PLLA peak and three peaks related to PCL segments[24]. Upon stretching and fixing at low temperature, the PLLA peak grew stronger, and the PCL peaks fused to form a new peak. We proposed that the alternation in WAXS was due to the oriented crystalline structure

induced by stretching. Meanwhile, the isotropic circle in the SAXS pattern changed into the diamond-shape ellipse, which verified the generation of stretch-induced crystalline structure. In the recovery state, the oriented crystalline structure in WAXS was still preserved, and an extra peak related to crystalline PLLA emerged. This PLLA peak might be generated during the stretching state, but show up in the recovery state owing to the time delay in WAXS data collection per shot. On the basis of the above patterns, we could rationalize the magnificent shape fixing ratio of PCL80LL20 by the well-preserved stretch-induced crystalline structure of PLLA and PCL. Unfortunately, PCL80LL20 lost the virtue during shape recovery because the recovery of amorphous PCL segment was impeded by the oriented PCL-PCL crystalline domain. For PCL60LL40 at the initial state, the WAXS pattern revealed crystalline PLLA segment (at 13° and 16°). After extension, the circular shape in the SAXS pattern was converted to a diamond shape i.e. forming the oriented crystalline structure. Moreover, the WAXS peak at 16° was reduced and that at 13° was increased. These changes supported the formation of oriented crystalline PLLA shifting the (203) plane (16°) to predominantly (110)/(200) planes (13°). The strengthened diffraction peak at 13° may act as the fixing element for shape memory polyurethanes. In the meantime, the intensity of WAXS amorphous halo decreased because the oriented crystalline PLLA occupied the space of amorphous PCL segments. After heating to 50

°C, the SAXS and WAXS patterns of PCL60LL40 remained the diamond shape, indicating that the oriented crystalline structure was well preserved. These patterns could explain the better shape memory properties of PCL60LL40. In another words, the fixing capability of the oriented PLLA-PLLA crystalline domain was considered to restrain the tendency of elastic recoiling, and the amorphous PCL segment rebound without being hindered by the crystalline PLLA. Schematics that summarize the different behaviors of PCL100, PCL80LL20, and PCL60LL40 are displayed in Figure S5.

The possible shape memory mechanism of PCL/PLLA-based polyurethanes is summarized in Figure 7A. The PLLA crystals showed random direction, and the amorphous PCL was soft before stretching. Upon deformation, the crystalline PLLA structure was elongated and oriented by aligning to the extension direction. At the same time, PCL segments were also aligned and fixed. In the recovery state, the oriented crystalline PLLA was not affected by heating, while the amorphous PCL segments retracted to the initial flexible state. In the existing literature, the effect of "orientation" of crystalline structure on shape memory behavior has not been examined.

Since the waterborne polyurethane SME developed was intended for use in human body, the shape memory behavior in 37 °C water was further investigated.

Results showed excellent shape memory behavior of PCL60LL40 in 37 °C water, which was superior to that in the dry state. According to literature[25], the water molecule would diffuse into polyurethane chains to block the hydrogen bond. After PCL60LL40 was immersed in water, the fraction of hydrogen-bonded C=O (1643 cm^{-1}) decreased and the absorbance of N-H band (near 3360 cm^{-1}) was also lower. We suggested that the amounts of hydrogen bond between C=O and N-H in the polymer possibly decreased as a result of water penetration. The hindered molecular bonding and lubrication effect of water was also supported by the lower mechanical strength and higher elongation of the polymer in the wet state. Because the secondary force in the polymer became smaller, the energy required to recover might be less. Thus, PCL60LL40 could recover to 100% in 37 °C water. The possible mechanism for improved shape memory PCL60LL40 in water is illustrated in Figure 7B. When the PLLA segments were stretched to establish a closely packing crystalline structure, the secondary force (hydrogen bond and van der Waal force) became stronger to fix the deformed shape. Upon recovery, water molecules could interfere with the oriented structure, weakening the molecular interaction in the stretched polyurethane. The crystallized polymer chains might also be lubricated by the diffused water molecules. Therefore, the polyurethane recovered to the initial state faster and more completely in 37 °C water than that in 50 °C air. To verify water diffusion, we investigated the

effect of water immersion on the crystallinity and contact angle of PCL60LL40 (Figure S9). The decreases in crystallinity and contact angle supported that the water could diffuse into the soft segment of waterborne polyurethane.

Vascular ECs play an important role in preventing blood clotting[26]. Cardiovascular devices should facilitate the growth of ECs to achieve endothelialization. The biological evaluation in this study confirmed the potential of PCL60LL40 in blood-contacting applications. The EC proliferation and blood compatibility appeared to be enhanced by the addition of PLLA segments. PLLA has better cell affinity than PCL [27] and has been used in biodegradable vascular stents [28]. Therefore, PCL60LL40 with the highest PLLA content displayed the best EC proliferation and least platelet activation. The good cell viability on PCL60LL40 might also be owing to the more hydrophilic surface. Besides, the crystallinity of PLLA soft segment may lead to a greater extent of microphase separation of the polyurethane, which has been associated with the biocompatibility of polyurethanes [29]. With the highest PLLA crystallinity, PCL60LL40 had the best proliferation of ECs and the least activation of platelets among the prepared samples. Although the commercial Pellethane displayed greater cytocompatibility than biodegradable polyurethanes synthesized in this study, the extent of platelet activation on Pellethane

was much greater. Besides, Pellethane is not biodegradable and does not possess shape memory behavior.

In summary, biodegradable polyurethane elastomer developed in this work was equipped with shape memory ability near 37°C. Through in situ SAXS/WAXS measurements, the oriented PLLA structure was considered as the fixing element, and the amorphous PCL oligodiol was responsible for recovery. The optimized shape memory polyurethane (PCL60LL40) was degraded by 10% under 37ºC in PBS solution after 28 days. Both PCL and PLLA oligodiols that we selected are well-known biodegradable polymers. Because the related polymers are degraded by pure hydrolysis[30], we estimate that the polymer would be fully degraded in 6-12 months in vivo, depending on the implantation site. The biodegradable polyurethane shape memory elastomer also exhibited low platelet activation and proliferation of ECs. These properties make it suitable for applications such as cardiovascular devices and tissue engineering scaffolds.

5. Conclusions

We developed a series of PCL-PLLA based biodegradable polyurethanes as shape memory elastomers by a waterborne method. The optimized polyurethane, PCL60LL40 (soft segment PCL:PLLA 6:4) had ~10% lamellar crystalline structure

and good shape memory properties. The mechanism for shape memory was elucidated by in situ SAXS/WAXS measurements. The recovery segments were the amorphous PCL segments, and the stretch-induced crystalline PLLA acted as the fixing segments. The two-dimensional SAXS pattern of PCL60LL40 revealed a clear diamond shape, indicating the formation of oriented structure. The shape recovery ratio of PCL60LL40 in 37 °C water approached nearly 100% and the recovery was very fast, probably because water molecule could penetrate rapidly into the oriented crystalline structure and interfere with the hydrogen bond of the polymer chains. The biodegradable polyurethane shape memory elastomer developed in this study also demonstrated good biocompatibility and low platelet activation. This smart heat and water responsive shape memory elastomer may have potential biomedical applications.

Acknowledgments

This work was supported by the Program of Additive Manufacturing (MOST 104-2218-E-002-010), Ministry of Science and Technology, Taiwan, R.O.C.

Supporting information

The synthesis process, the thermal properties, the XRD and SAXS profiles, the average platelet adhesion and activation, the stress-strain curves, and the ATR-IR spectra of all polyurethanes. This material is available free of charge via the Internet at http://pubs.acs.org/.

References

(1) Liu, C.; Qin, H.; Mather, P. Review of Progress in Shape-memory Polymers. *J. Mater. Chem.* 2007, 17, 1543-1558.

(2) Yakacki, C. M.; Shandas, R.; Safranski, D.; Ortega, A. M.; Sassaman, K.; Gall, K. Strong, Tailored, Biocompatible Shape-Memory Polymer Networks. *Adv. Funct. Mater.* 2008, 18, 2428-2435.

(3) Hampikian, J. M.; Heaton, B. C.; Tong, F. C.; Zhang, Z.; Wong, C. Mechanical and Radiographic Properties of a Shape Memory Polymer Composite for Intracranial Aneurysm Coils. *Mater. Sci. Eng., Part C* 2006, 26, 1373-1379.

(4) Krueger, U.; Zanow, J.; Scholz, H. Computational Fluid Dynamics and Vascular Access. *Artif. organs.* 2002, 26, 571-575.

(5) Small IV, W.; Metzger, M. F.; Wilson, T. S.; Maitland, D. J. Laser-activated Shape Memory Polymer Microactuator for Thrombus Removal following Ischemic Stroke: preliminary in Vitro Analysis. *IEEE J. Quantum Electron.* 2005, 11, 892-901.

(6) Lendlein, A.; Langer, R. Biodegradable, Elastic Shape-memory Polymers for potential Biomedical Applications. *Science.* 2002, 296, 1673-1676.

(7) Zhang, D.; George, O. J.; Petersen, K. M.; Jimenez-Vergara, A. C.; Hahn, M. S.; Grunlan, M. A. A Bioactive "Self-fitting" Shape Memory Polymer Scaffold with Potential to treat Cranio-maxillo Facial Bone Defects. *Acta Biomater.* 2014, 10, 4597-4605.

(8) Lendlein, A.; Schmidt, A. M.; Langer, R., AB-polymer Networks based on Oligo (ε-caprolactone) Segments showing Shape-Memory Properties. *Proc. Natl. Acad. Sci.* 2001, 98, 842-847.

(9) Lendlein, A.; Jiang, H.; Jünger, O.; Langer, R. Light-induced Shape-memory Polymers. *Nature.* 2005, 434, 879-882.

(10) Han, X. J.; Dong, Z. Q.; Fan, M. M.; Liu, Y.; Wang, Y. F.; Yuan, Q. J.; Li, B. J.; Zhang, S. pH-Induced Shape-Memory Polymers. *Macromol. Rapid Commun.* 2012, 33, 1055-1060.

(11) Chae Jung, Y.; Hwa So, H.; Whan Cho, J. Water-Responsive Shape Memory Polyurethane Block Copolymer Modified with Polyhedral Oligomeric Silsesquioxane. *J. Macromol. Sci., Part B* 2006, 45, 453-461.

(12) Cho, J. W.; Kim, J. W.; Jung, Y. C.; Goo, N. S., Electroactive Shape-memory Polyurethane Composites incorporating Carbon Nanotubes. *Macromol. Rapid*

Commun. 2005, 26, 412-416.

(13) Meng, Q.; Hu, J. A Aeview of Shape Memory Polymer Composites and Blends. *Composites Part A* 2009, 40, 1661-1672.

(14) Ratna, D.; Karger-Kocsis, J. Recent Advances in Shape Memory Polymers and Composites: A Review. *J. Mater. Sci.* 2008, 43, 254-269.

(15) Miaudet, P.; Derré, A.; Maugey, M.; Zakri, C.; Piccione, P. M.; Inoubli, R.; Poulin, P., Shape and Temperature Memory of Nanocomposites with Broadened Glass Transition. *Science.* 2007, 318, 1294-1296.

(16) Hawkins, W. L. Polymer Degradation and Stabilization. *Springer*. 1984; Berlin.

(17) Cha, K. J.; Lih, E.; Choi, J.; Joung, Y. K.; Ahn, D. J.; Han, D. K. Shape-Memory Effect by Specific Biodegradable Polymer Blending for Biomedical Applications. *Macromol. Biosci.* 2014, 14, 667-678.

(18) Cohn, D.; Stern, T.; González, M. F.; Epstein, J. Biodegradable Poly (ethylene oxide)/poly (ε-caprolactone) Multiblock Copolymers. *J. Biomed. Mater. res.* 2002, 59, 273-281.

(19) Hsu, S.h.; Hung, K.C.; Lin, Y.Y.; Su, C.H.; Yeh, H.Y.; Jeng, U.S.; Lu, C.Y.; Dai, S. A.; Fu, W.-E.; Lin, J.-C. Water-based Synthesis and Processing of novel Biodegradable Elastomers for Medical Applications. *J. Mater. Chem. B* 2014, 2, 5083-5092.

(20) Takahashi, T.; Hayashi, N.; Hayashi, S., Structure and Properties of Shape-Memory Polyurethane Block Copolymers. *J. Appl. Polym. Sci.* 1996, 60, 1061-1069.

(21) Ou, C.W.; Su, C.H.; Jeng, U.S.; Hsu, S.h. Characterization of Biodegradable Polyurethane Nanoparticles and Thermally induced Self-assembly in Water Dispersion. *ACS Appl. Mater. Interfaces.* 2014, 6, 5685-5694.

(22) Ryuji I.; Masaya K.; Seeram R., Structure and Properties of Electrospun PLLA single Nanofibers. Nanotechnology, 2005, 16, 208-213.

(23) Zhou, H.; Wilkes, G. Comparison of Lamellar Thickness and its Distribution determined from D.S.C., SAXS, TEM and AFM for High-density Polyethylene Films having a stacked Lamellar Morphology. *Polymer.* 1997, 38, 5735-5747.

(24) Jeong, J. H.; Kang, H. S.; Yang, S. R.; Kim, J.D., Polymer Micelle-like aggregates of novel Amphiphilic Biodegradable Poly (asparagine) grafted with Poly (caprolactone). *Polymer.* 2003, 44, 583-591.

(25) Huang, W.; Yang, B.; An, L.; Li, C.; Chan, Y., Water-driven Programmable Polyurethane Shape Memory Polymer: Demonstration and Mechanism. *Appl. Phys. Lett.* 2005, 86, 114105.

(26) Pearson, J. D. Endothelial Cell Function and Thrombosis. *Best Pract. Res. Clin. Haematol.* 1999, 12, 329-341.

(27) Patrício T.; Domingos M.; Gloria A.; Bártolo P., Characterisation of PCL and

PCL/PLA Scaffolds for Tissue Engineering. *Procedia CIRP*. 2013, 5, 110-114.

(28) Ashton J.H.; Mertz J.A.M.; Harper J.L.; Slepian M.J.; Mills J.L.; McGrath D.V.; Vande Geest J.P., Polymeric Endoaortic Paving: Mechanical, Thermoforming, and Degradation Properties of Polycaprolactone/polyurethane Blends for Cardiovascular Applications. *Acta Biomaterialia*. 2011, 7, 287-294.

(29) Takahara A.; Tashita J.; Kajiyama T.; Takayanagi M., Microphase Separated Structure, Surface Composition and Blood Compatibility of Segmented Poly(urethaneureas) with Various Soft Segment Components. *Polymer*, 1985, 26, 987-996.

(30) Choi N.S.; Kim C.H.; Cho K.Y.; Park J.K. Morphology and Hydrolysis of PCL/PLLA Blends compatibilized with P(LLA-co-εCL) or P(LLA-b-εCL). *J. Appl. Polym. Sci.* 2002, 86, 1892-1898.

Tables

Table 1. Thermal properties and crystallinity measured by DSC and XRD.

Polyurethane samples	DSC				XRD
	Tg (°C)	Tm (°C)	Heat flow (J/g)	Crystallinity (%)	Crystallinity (%)
PCL60LL40	-	126.29	5.52	5.93	10.52
PCL80LL20	-	45.85	5.829	4.29	10.94
PCL100	-49.49	-	-	-	-

PCL60LL40 represents the polyurethane sample of which the soft segment contained 60 mol% PCL and 40 mol% PLLA. PCL80LL20 represents the polyurethane sample of which the soft segment contained 80 mol% PCL and 20 mol% PLLA. PCL100 represents the polyurethane sample of which the soft segment contained 100 mol% PCL.

Table 2. Shape fixity ratios and shape recovery ratios for various polyurethanes. Recovery was performed at 50°C air. Shape memory procedure: refer to text and Figure 2.

Polyurethane samples	Cycle 1		Cycle 2	
	R_{f1} (%)	R_{r1} (%)	R_{f2} (%)	R_{r2} (%)
PCL100	36±3.4	100±0.0	41.6±7.1	88.8±2.3
PCL80LL20	100±0.0	38.8±7.5	100±0.0	28±3.5
PCL60LL40	74.5±5.0[a]	87.2±3.8[b]	80.5±5.2[a]	85.9±4.4[b]

[a] $p < 0.01$ between PCL60LL40 and PCL100.

[b] $p < 0.001$ between PCL60LL40 and PCL80LL20.

R_{f1}: the fixity ratio in Cycle 1.

R_{r1}: the recovery ratio in Cycle 1.

R_{f2}: the fixity ratio in Cycle 2.

R_{r2}: the recovery ratio in Cycle 2.

Table 3. Shape recovery ratios and times of PCL60LL40 in different recovery conditions.

Recovery condition	Shape recovery ratio (%)	Shape recovery time (s)
Air 50°C	87.2±3.8	72.3±4.1
Air 37°C	71.3±3.1	80.6±4.0
Water 25°C	65.5±4.1	37.6±3.2
Water 37°C	100±0.0	16.3±2.3

Table of Contents Graphic

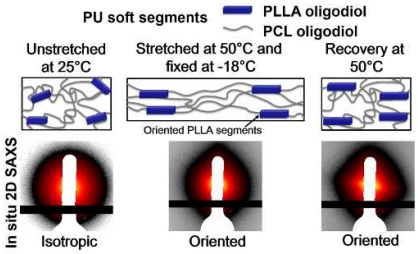

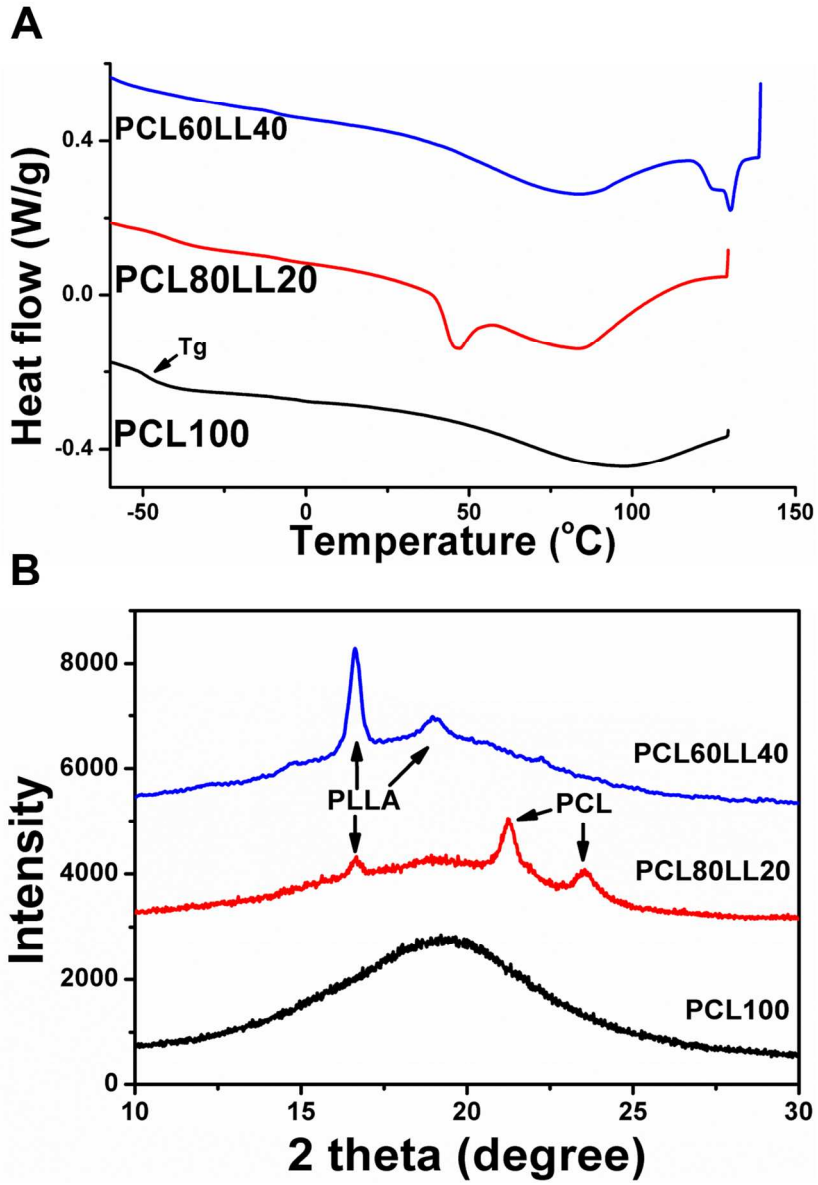

Figure 1. (A) DSC heating curves of PCL100, PCL80LL20, and PCL60LL40. The endothermic peaks at 45°C and 125°C stands for PCL and PLLA melting heat respectively. (B) XRD pattern of PCL100, PCL80LL20, and PCL60LL40. The peaks at 16.5° and 18.9° represents PLLA crystal, and the peaks at 21° and 23° represents PCL crystals.

314x453mm (300 x 300 DPI)

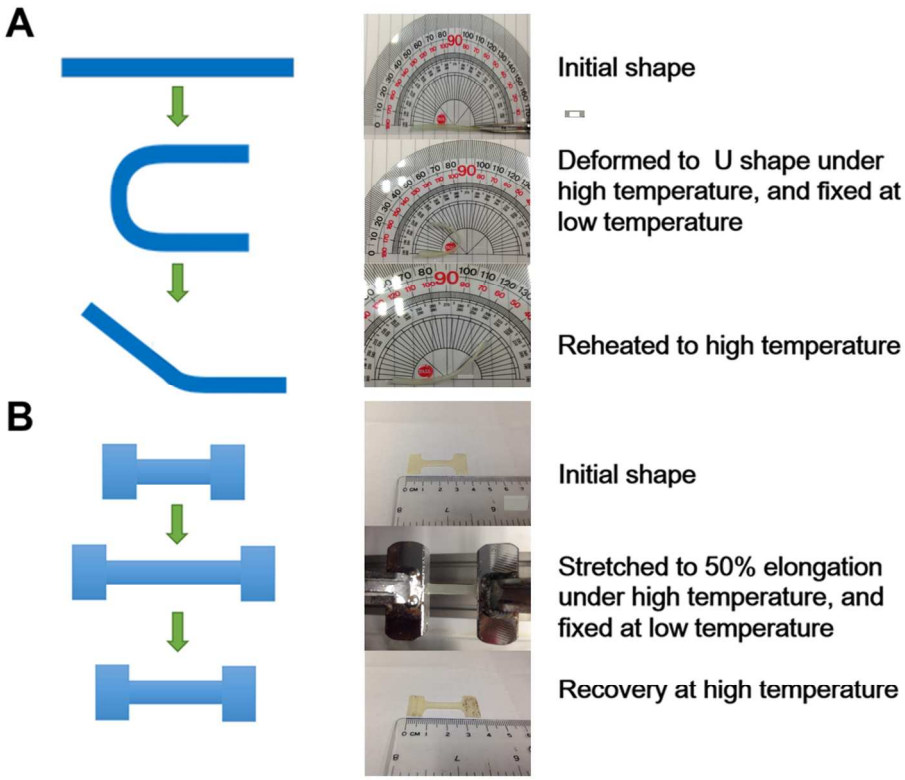

Figure 2. Shape memory processes for evaluation of shape memory indices and for the in situ WAXS/SAXS measurements. (A) The film [40 mm (length) × 5 mm (width) × 0.2 mm (thickness)] was flat before deformation. After being heated to a higher temperature, the film was deformed to U shape, and cooled to fix the temporary shape. Finally, the film recovered to the initial shape upon heating. Quantitative results of fixity and recovery ratios are summarized in Table 2. (B) For in situ WAXS/SAXS, the film [20 mm (length) × 4.7 mm (width) × 0.2mm (thickness)] was installed on the tensile tester and stretched to 50% elongation at 50°C, and cooled to -18°C fix the elongated shape. After fixing, the film was heated (50°C) to recover to the initial shape. Results collected from in situ WAXS/SAXS are shown in Figure 3.

423x339mm (300 x 300 DPI)

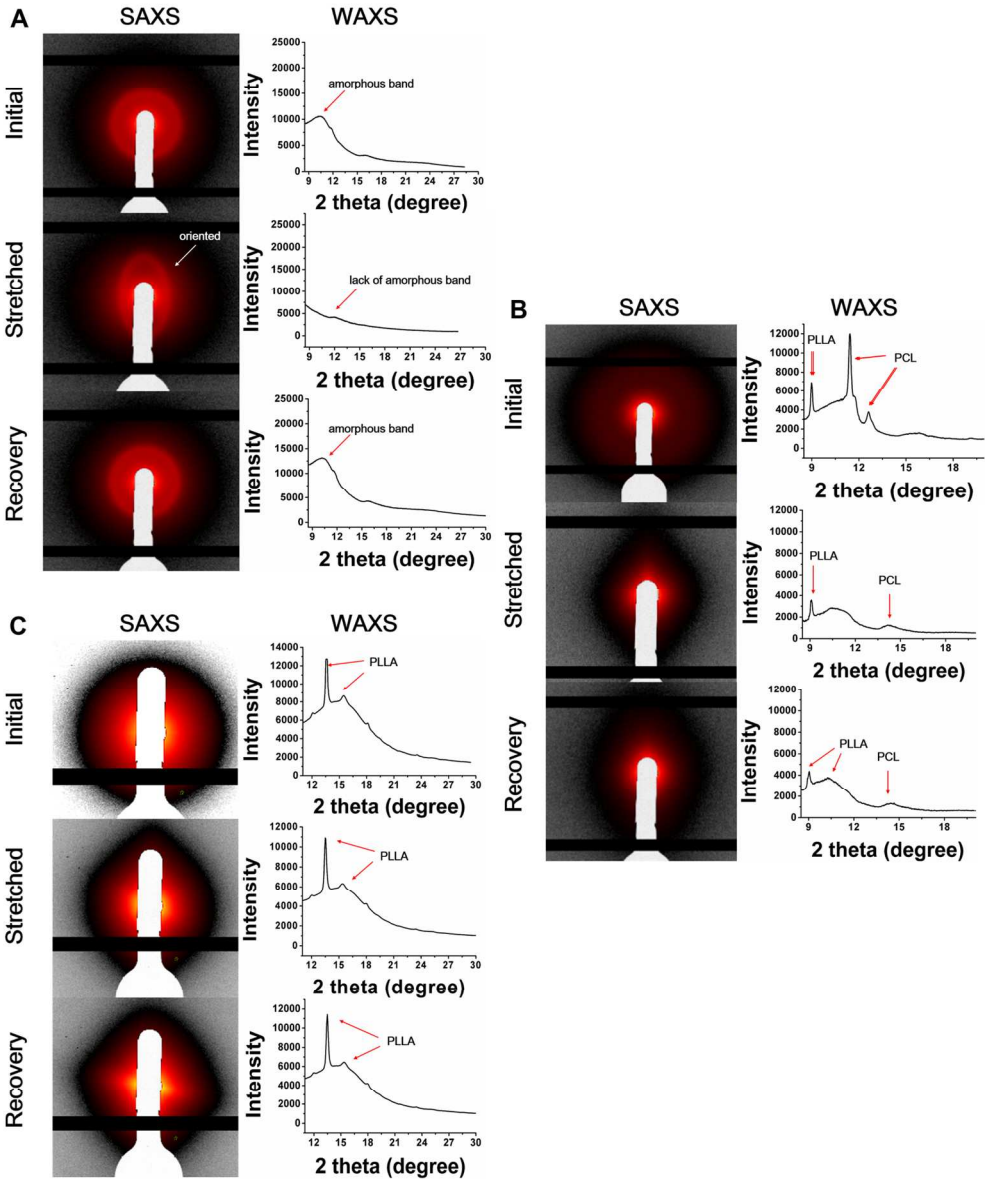

Figure 3. Two-dimensional (2D) SAXS and WAXS patterns collected during the in situ shape memory test. Polyurethane films were installed at the initial state under 25°C, stretched under 50°C to 50% strain, and cooled to -18°C to the fixing state. The films were then heated to 50°C to the recovery state. (A) PCL100, (B) PCL80LL20, (C) PCL60LL40.

445x539mm (300 x 300 DPI)

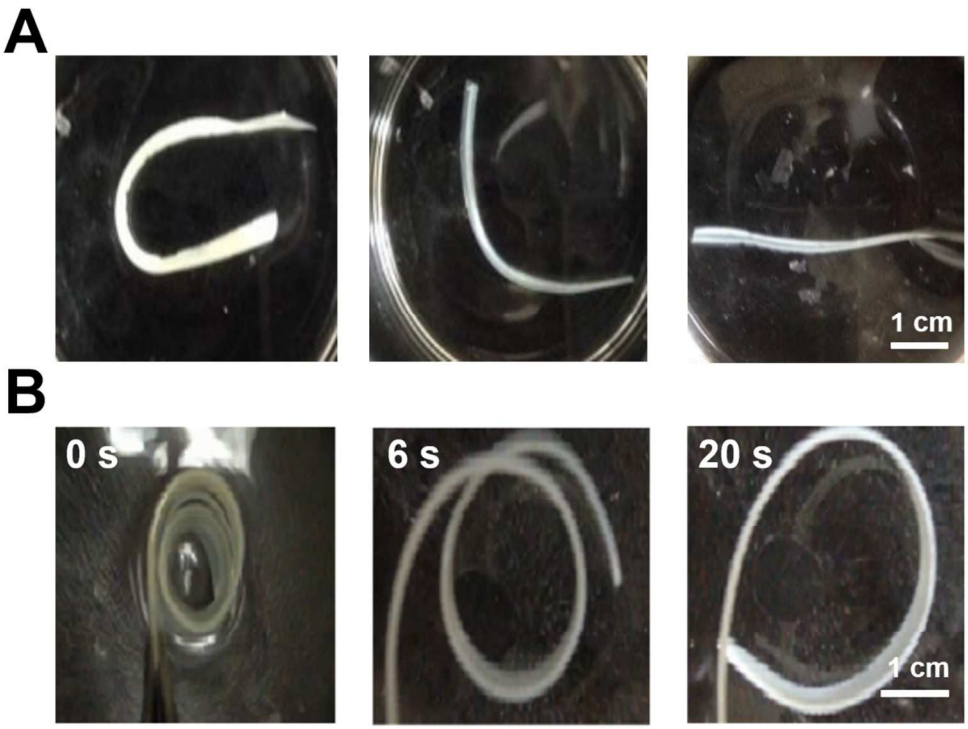

Figure 4. Shape recovery of PCL60LL40 in 37°C water. (A) The sample [40 mm (length) × 5 mm (width) × 0.2 mm (thickness)] was bended to U shape at 50°C, and then fixed at -18°C. Finally, the U shape film was put into 37°C water. Quantitative results of fixity and recovery ratios are summarized in Table 3. (B) The sample [80 mm (length) × 5 mm (width) × 0.2 mm (thickness)] was deformed to spiral shape at 50°C. The deformed shape was then fixed at -18°C. After fixing the sample was put into 37°C water. The fast recovery in 20 s is illustrated.

335x248mm (300 x 300 DPI)

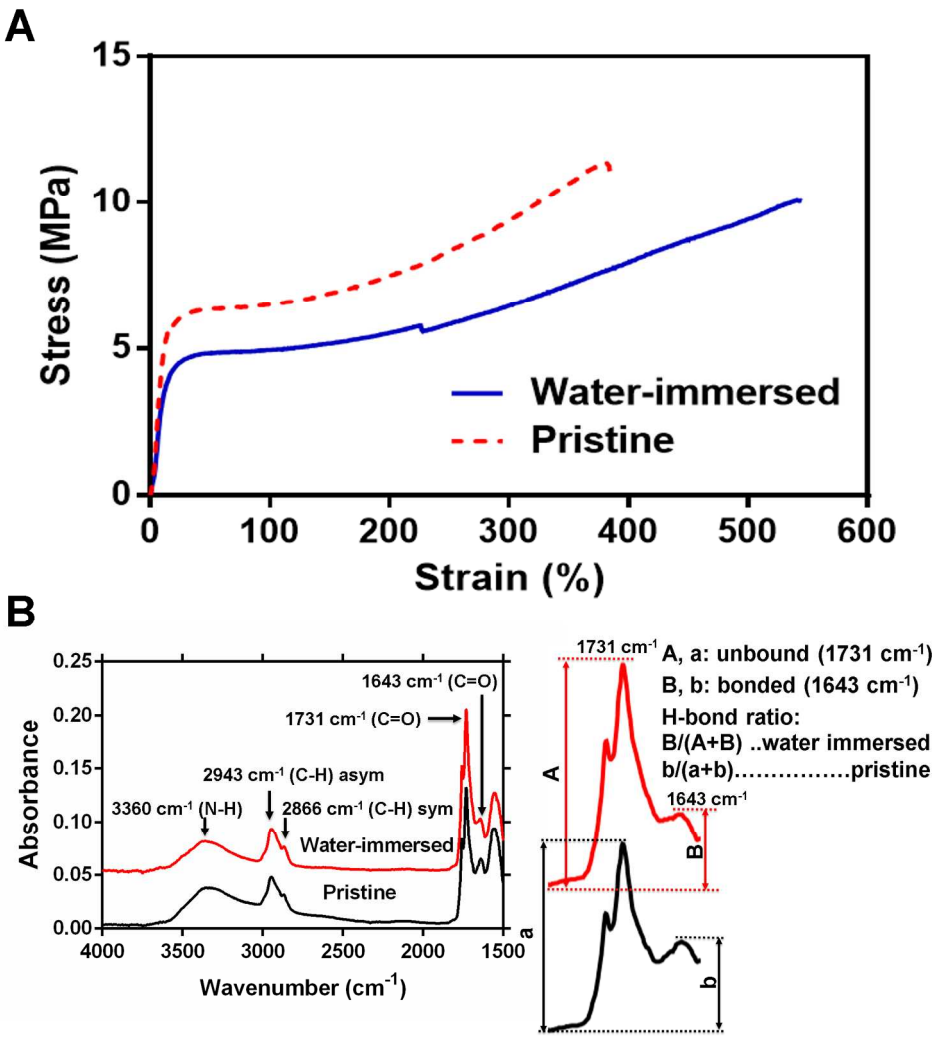

Figure 5. (A) Tensile stress-strain curves of PCL60LL40 at the testing speed of 100 mm/min (for elastomers), for the pristine and water-immersed samples. (B) ATR-IR spectra of PCL60LL40, for the pristine and water-immersed samples. Peaks at 1731 cm-1: unbound C=O. Peaks at 1643 cm-1: hydrogen-bonded (H-bonded) C=O. The pristine samples were the original dry films. The water-immersed samples were the films hydrated in water and then wiped off the surface water before measurement.

320x338mm (300 x 300 DPI)

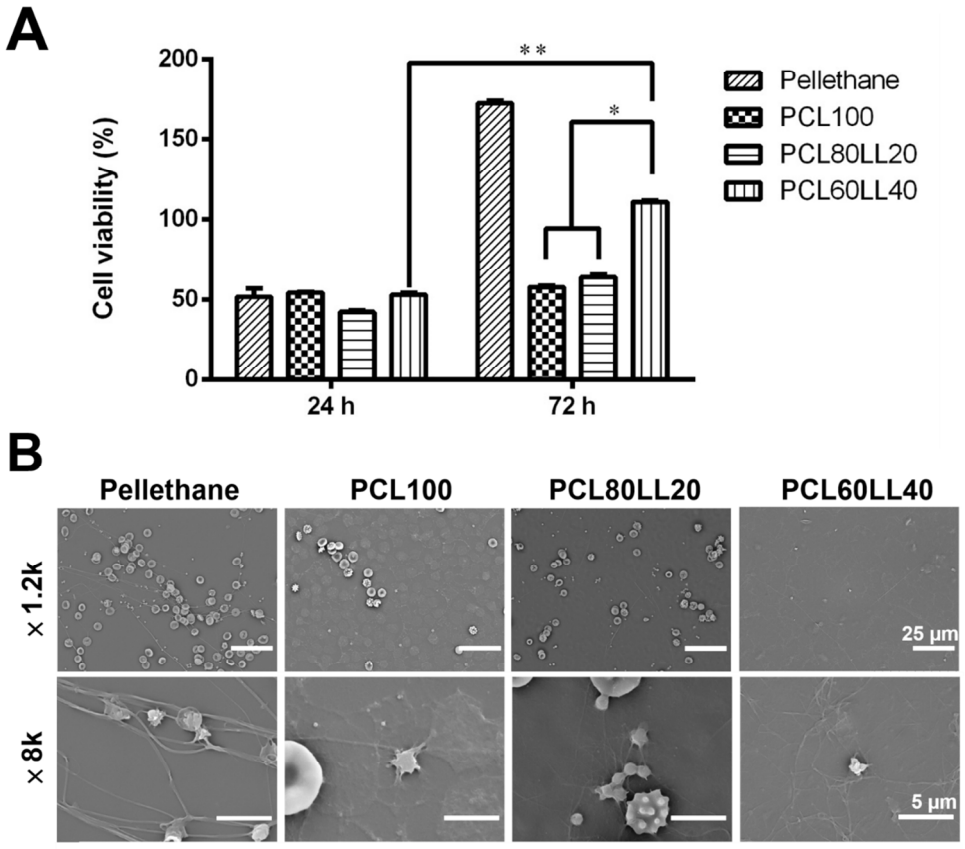

Figure 6. (A) Viability of endothelial cells (ECs) after incubation on various polyurethanes. Statistical significance: *p < 0.01 and **p<0.001. (B) Morphology of platelets on various polyurethanes.

335x297mm (300 x 300 DPI)

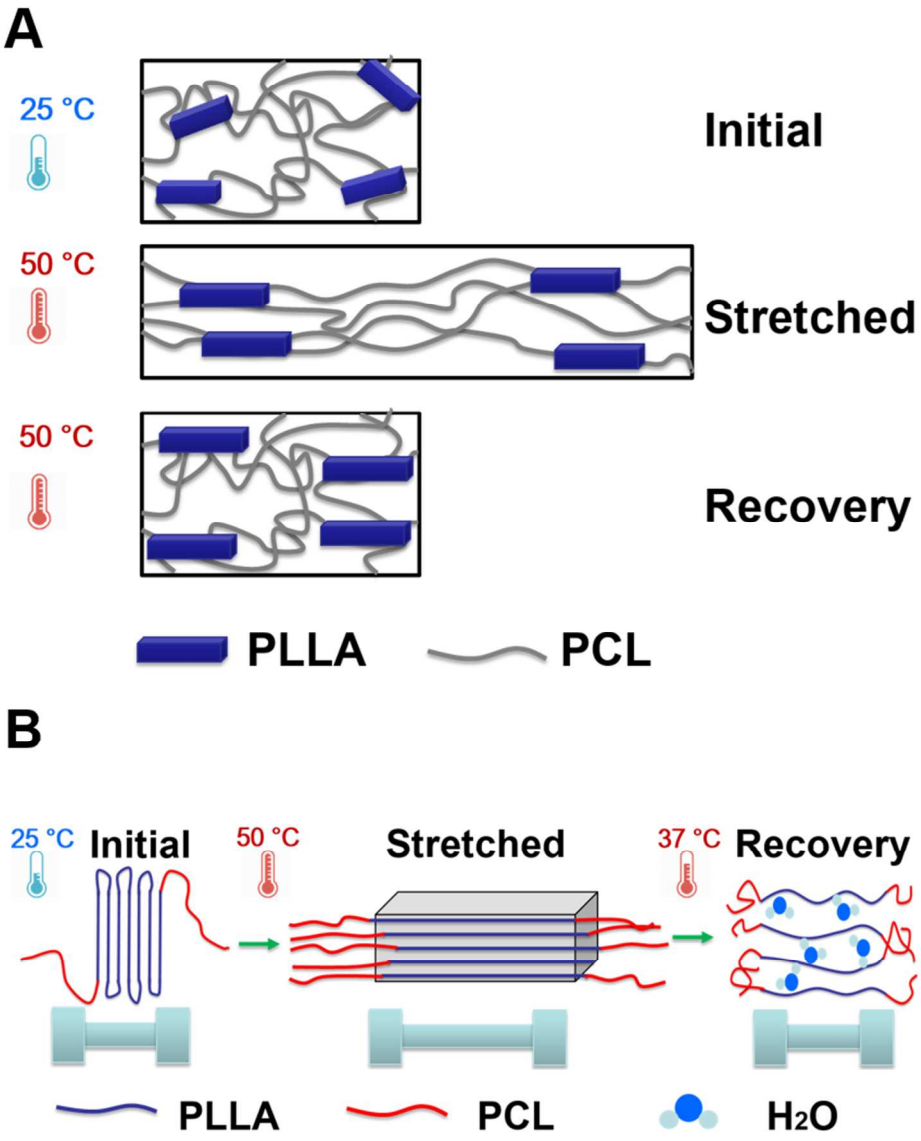

Figure 7. (A) Possible mechanism for the shape memory and recovery process under 50°C air. (B) Possible mechanism for the shape memory and recovery process in 37°C water.

236x292mm (300 x 300 DPI)